Title

Mechanisms of power dissipation in piezoelectric fans and their correlation with convective heat transfer performance

Authors

Ebrahimi, Navid Dehdari
Wang, Yide
Ju, Y Sungtaek

Publication Date

2018-04-01

DOI

10.1016/j.sna.2018.01.031

Peer reviewed

Mechanisms of Power Dissipation in Piezoelectric Fans and Their Correlation with Convective Heat Transfer Performance

Navid Dehdari Ebrahimi, Yide Wang, and Y. Sungtaek Ju*

Department of Mechanical and Aerospace Engineering
University of California, Los Angeles, CA 90095, USA
* corresponding author, email: just@seas.ucla.edu

Abstract

Piezoelectric fans offer an intriguing alternative to conventional rotary fans for thermal management of portable and wearable electronics due to their scalability, low power consumption and simple mechanical construct. We report a combined experimental and modeling study to help elucidate power dissipation mechanisms in piezoelectric fans. To analyze contributions from these different mechanisms, mathematical models that account for mechanical hysteresis, dielectric loss and viscous damping from generated air flows are used in conjunction with vibration amplitudes and power consumption data obtained experimentally from piezoelectric fans of different blade lengths, thicknesses and mass distributions. In parallel, we perform experiments on convective heat transfer coefficients and aerodynamic forces acting on surfaces that are oriented perpendicular with respect to fan-induced air flows. These experiments establish that the portion of power dissipation ascribed to air flows correlates well with the heat transfer performance and aerodynamic force. A power ratio, defined as the fraction of the air flow power to the total power dissipation, is then proposed as a useful indicator of the power efficiency of the piezoelectric fans. We show that the power efficiency exhibits a peak at a bias voltage amplitude that balances parasitic power dissipation, due in particular to mechanical hysteresis loss and the dielectric loss, with power dissipation directly linked to actual air flow generation. Lastly, we relate the air flow power to the blade's geometrical parameters to facilitate systematic optimization of the blades for both cooling performance and power efficiency.

Keywords: **electronics cooling, hysteresis loss, piezoelectric fan, power efficiency, wearable electronics**

1. INTRODUCTION

Recent development in portable and wearable electronics with limited access to power sources has led to challenges in their thermal management. Conventional rotary fans are difficult to scale down and are power inefficient when miniaturized. Piezoelectric fans are a promising alternative because of their simpler structures, less noise, and lower power consumption [1]–[3]. Piezoelectric fans typically consist of flexible blades attached to ceramic actuation beams. When operated near its resonance frequency, the blade undergoes large-amplitude vibrations, which in turn generate net airflows in the forward direction and induce convective heat transfer.

The fluid dynamics of vibrating beams has been widely investigated in the past. For example, Kim et al. [4] studied flow fields generated by vibrating beams using the particle image velocimetry and smoke visualization techniques. Eastman et al. [5] studied thrust forces generated by the motion of an oscillating cantilever beam over a wide range of Reynolds numbers and proposed a correlation relating the thrust to the vibration amplitude and frequency. The effects of solid sidewalls on the amplitude and resonance frequency of a piezoelectric beam were examined by Eastman and Kimber [6]. Interactions among piezoelectric fans operating in the vicinity of each other was studied in [7].

Past studies [8]–[16] also examined the effects of various parameters on the heat transfer performance of piezoelectric fans. These parameters include the gaps between blade tips and surrounding surfaces; the relative thickness and mechanical modulus of piezoelectric and blade materials; the blade length and width; and the amplitude and frequency of vibration. Huang et al. [17] used 3D numerical simulation in conjunction with an inverse design technique to determine the optimum position of a fan blade for maximum heat transfer performance. A similar approach was used to find the optimal positions and phase angle of a dual piezoelectric fan assembly [18]. Petroski et al. [19] attempted to tailor air flows created by piezoelectric fans using complex

geometric features to improve cooling performance. Local and average mass transfer coefficients were measured using the naphthalene sublimation technique in [20].

Power consumption is an important aspect of piezoelectric fans. Liang et al. [21] reported an impedance method for calculating electrical power dissipation in piezoelectric beams. Cho et al. [22] extended this work and developed a five-port equivalent electric circuit model, where power dissipation in piezoelectric bimorphs was represented in terms of equivalent electric impedances. Wait et al. [23] experimentally studied the electromechanical coupling factors (EMCF) of piezoelectric fans and concluded that the highest EMCF could be achieved at the 1st resonant natural frequency as opposed to higher-order resonant frequencies. The EMCF is a measure of the efficiency of the fans in converting electrical energy to mechanical energy.

Electrical losses, however, represent only a portion of power dissipation in piezoelectric fans. Mechanical losses due to mechanical hysteresis in shims and interfacial bonding materials, for example, can be appreciable. In a related study, Sheu et al. [24] observed that the hardness and thickness of bonding materials can have significant effects on vibration amplitudes.

Despite many past studies on piezoelectric fans, detailed understanding of their power dissipation mechanisms and power efficiency has been rather lacking. In the present work, we aim to improve our understanding of the power efficiency of convective cooling by piezoelectric fans and provide a guideline for selecting optimal fan operating condition.

We examine three main sources of power dissipation: dielectric loss within a piezoelectric actuator; mechanical hysteresis loss; and viscous dissipation in induced airflows. We use independently validated mechanical models together with experimentally measured data to estimate the contribution from each source of power dissipation. Convective heat transfer coefficients and normal forces due to the fan's operation are then correlated with the component of power directly related to induced air flows, referred to as air flow power. An optimal bias voltage for power efficiency, as characterized by the ratio of the air flow power to the total consumed power, is then determined using our model. Lastly, we relate the air flow power, and hence indirectly the heat transfer coefficient and normal force, to the blade's geometrical parameters to facilitate systematic optimization of the blades for both cooling performance and power efficiency.

2. Experimental Setup

We use commercial piezoelectric fans (Steminc, Inc.) modified in-house for the present study. The piezoelectric actuator in each of the fans consists of two 185 μm-thick piezoelectric ceramic film (Pb ($Zr_{0.53}Ti_{0.47}$) O_3; PZT - 4) with a 142 μm-thick copper shim sandwiched in between. The other geometric parameters of the piezoelectric fans (Fig. (1)) and their natural resonant frequencies are listed in Table 1. The blades of different thicknesses are made by bonding different numbers of Kapton sheets, each with a thickness of 0.127 mm. The blade width w_b is kept 12 mm. The actuators are clamped at the base to realize a cantilever configuration, as confirmed optically from the negligible slope of the actuator base during operation.

We use a high-speed camera with a maximum frame rate of 16000 fps and a video zoom lens to measure the amplitude of both blade and actuator vibrations. The uncertainty in the measured vibration amplitudes is estimated to be approximately 7 μm, representing less than 5% of the typical values of the measured vibration amplitudes of the actuator. The mechanical hysteresis and structural damping in piezoelectric fans is characterized in a vacuum chamber at a pressure of approximately 1cm Hg where the effects of aerodynamic damping can be neglected [25].

A function generator (Model 33220A, Agilent) is used to generate small amplitude (0.4V - 2V) pure sinusoidal voltage waves, which are then amplified using a high-voltage amplifier with a current monitor output (Model PZD700A, TREK). The uncertainty due to voltage and current measurements are estimated to be 2 V and 0.041 A, or approximately 2% and 7% in typical measurements. The total power dissipation in a piezoelectric fan is obtained by numerically integrating the product of the measured voltage and current profiles (sampling rate 5000 Hz), with an estimated uncertainty of 0.5 mW, approximately 8% of typical measured powers.

Fig. (2.a) schematically shows our experimental setups to characterize the heat transfer coefficient and normal aerodynamic force on flat surfaces. Convective heat transfer coefficients over a flat surface are measured using an aluminum block (2.5 cm × 2.5 cm × 0.48cm) that has a thin-film electric heater of the same lateral dimensions attached to its back. The aluminum block-heat assembly is enclosed in a Styrofoam insulation to minimize parasitic heat loss through the side and back surfaces. The front surface of the aluminum block is coated with a black paint (Kylon Colormaster No.1602) to achieve uniform controlled emissivity. Five K-type thermocouples are attached to the aluminum block at four corners and in the middle to monitor its temperature (Fig. (2.b)). The spatial variations in the measured temperature rises, relative to the ambient temperature, are less than 5%. For all the experiments reported in the present manuscript, we keep the distance of the fan blade tip to the heated surface constant at 20 mm. The major paths of heat loss are conduction through the insulation layer on the back and side surfaces and radiation from the heated front surface. Heat loss is thus estimated by knowing the emissivity of the coating on the front surface and measuring the temperature profile of the back and side surfaces, using $Q_{loss} = [\int k_{ins} (T_i - T_o(x,y))/l \, dS] + [\varepsilon\sigma S(T_s^4 - T_\infty^4)]$. ε is the emissivity of the coating on the aluminum surface (0.95), σ is the Stephan-Boltzmann constant, S is the area of the heated surface, T_o , T_s and T_∞ are the insulation temperature, front surface temperature and the room temperature respectively. The estimated total heat loss rate is 1.35 W, approximately 45% of the typical heater power used in the present study, 32% of which is due to radiation from the front surface. The values of total (combined free and forced) convection is then calculated from $h_{total} = (Q_{heater} - Q_{loss})/S(T_s - T_\infty)$. The reliability of the estimated values of h_{total} is validated by comparing the experimental results obtained for natural convection (with the fan being off) with the existing empirical correlations where we observed good agreement within 10% over the range of

surface temperatures relevant to this study. The estimated uncertainties in total heat transfer coefficients and Nusselt numbers are ~3 W/m^{2}K and 5, respectively, approximately 12% of the typical values.

A weight scale (Model Adventurer Pro, Ohaus) with a resolution of 0.0001 g is used to measure the force exerted by a piezoelectric-fan-generated airflow on an opposing flat surface (Fig. (2.c)).

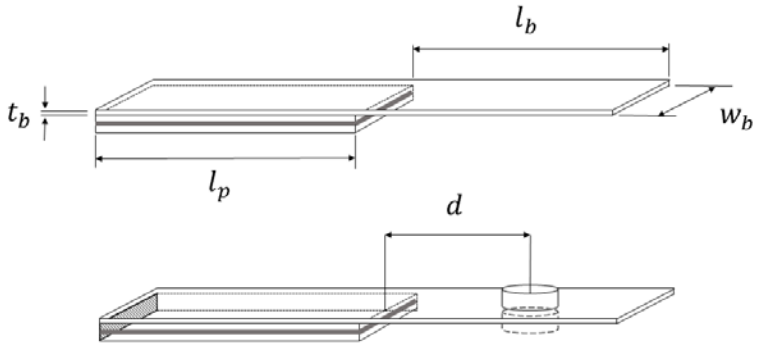

Fig. 1. The length (l_b), the thickness (t_b) and the location of the center of mass (d) of the blades are varied in different sets of experiments. The width of the blade is fixed.

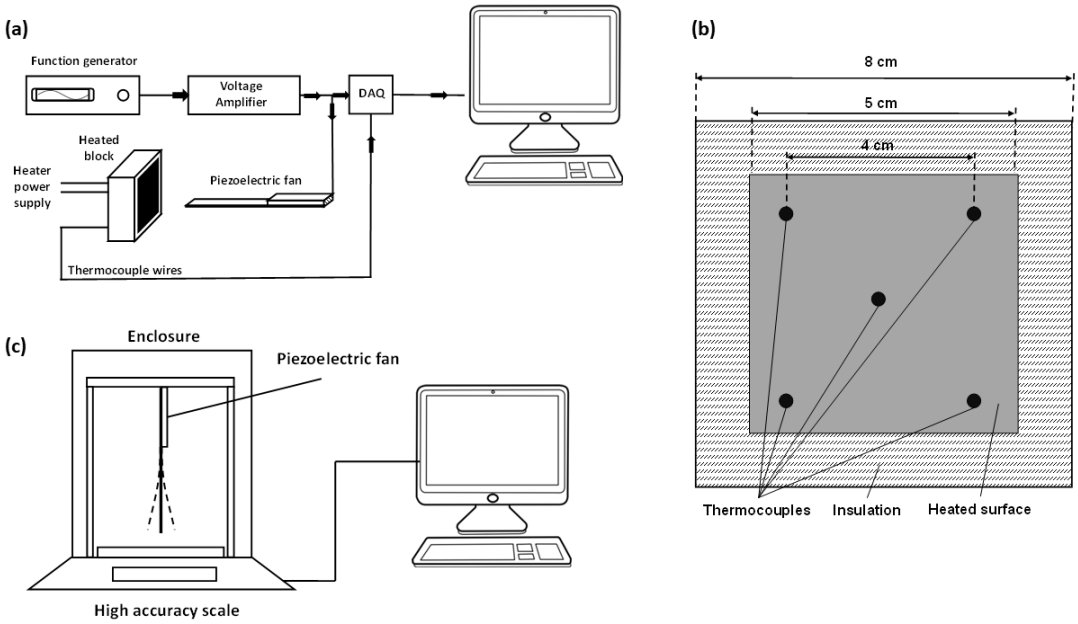

Fig. 2. Schematic of a) the heat transfer and power measurement setup, b) the exact location of the thermocouples and c) the aerodynamic force measurement setup used in the present study.

3. MODELS FOR POWER DISSIPATION

3.1. Piezoelectric bimorph actuators

Actuators often used in piezoelectric fans are bimorph cantilevers with a metal shim sandwiched between two piezoelectric layers. In a piezoelectric fan operating at its resonance frequency, a considerable portion of power can be consumed in the actuator itself. We first consider power dissipation in the actuator, which can be divided into two main categories: 1) electrical losses and 2) mechanical losses. The electrical loss is due primarily to dielectric loss in the piezoelectric materials [26] whereas the mechanical loss is due to hysteresis loss in the shim and bonding layers [21] [24] and structural damping.

The dielectric loss is calculated using

TABLE 1
EXPERIMENT VARIABLES

Control variable	l_b (mm)	t_b (mm)	d (mm)	Frequency (Hz)	Voltage amplitude (V)
blade length	63 - 20	0.26	-	30 - 188	70 - 140
blade thickness	32	0.13 - 0.5	-	35 - 119	70 - 140
location of mass	32	0.26	0 (no extra mass) - 17	62 - 20.7	50 - 190

$$P_{dielectric} = V_{rms}^2 \, Re(Y) \tag{1}$$

where Y is the electrical admittance of the piezoelectric material and V_{rms} is the RMS value of the applied sinusoidal voltage. The admittance in turn is a function of the tangent loss factor, $tan\ \delta = j2\pi f[\varepsilon_r \varepsilon_0 (1 - j \tan \delta)] \frac{l\,w}{2t}$. Here f, ε_r and ε_0 are the frequency, the dielectric constant and the vacuum permittivity, respectively. l, w, and t are the length, width and thickness of the piezoelectric material, respectively. We use the values reported in the literature for the tangent loss factor of the piezoelectric material used in the present study (PZT-4) [27], [28].

To quantify power dissipation due to mechanical hysteresis, we adapt a model reported by Low and Gou [29]. They introduce a state variable z, coupled with the equation of motion of the actuator:

$$\begin{aligned} \dot{z} &= \alpha_p d_e \dot{V} - \beta_p |\dot{V}| z - \gamma_p \dot{V} |z| \\ m_{e,1}\ddot{y} + C_1 \dot{y} + k_1 y &= k_1 (d_e V - z) \end{aligned} \tag{2}$$

Here, α, β and γ are parameters related to the shape of the hysteresis loop, V is the excitation voltage amplitude, $m_{e,1}$ is the effective mass of the actuator (= 33/140 m_0), k_1 is the mechanical stiffness of the actuator beam, and F_0 is the equivalent force applied to the tip of the actuator. m_0 is the mass of the actuator and C_1 is the structural damping coefficient for the actuator.

For sinusoidal bias voltages and the ranges of vibration amplitudes considered in the present study, the model can be well-approximated by replacing the terms $k_1 d_e V$ and $k_1 z$ in Eq. (2) with the equivalent force F_0 due to bending of the actuator at the tip and the hysteresis parameter H, respectively (Appendix B).

$$m_{e,1}\ddot{y} + C_1 \dot{y} + k_1 y + H\ sign\ (\dot{y}) = F_0 sin(\omega t) \tag{3}$$

Fig. (3) shows the schematic representation of the mechanical model captured in Eq. (3).

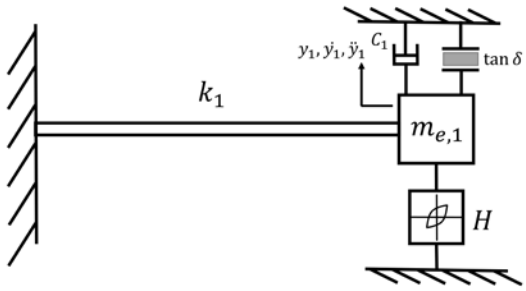

Fig. 3. Schematic of the proposed mechanical model for the piezoelectric bimorph actuator that accounts for mechanical hysteresis (H) and structural damping (C_1).

The hysteresis parameter H has the unit of force and can be interpreted as a measure of the opposing force arising from mechanical hysteresis under harmonic excitation [24], [29]. Its magnitude can be determined from a mechanical hysteresis loop, an example of which is shown in Fig. (4). We note that the piezoelectric fans are operated near the resonance frequencies of the blades (20 ~ 120 Hz). These are well below the resonant frequency of the actuator (~300 Hz), around which rate dependency of hysteresis causes significant deviation from quasi-steady condition [30]–[32]. The hysteresis loop is approximated using a parallelogram that conserves the area [30]. The intersections of the parallel top and bottom sides of the parallelogram with the displacement axis, labeled z^+ and z^-, are multiplied by mechanical stiffness of the actuator k_1 to determine H. The values of H determined using this

method for the current actuators are listed in Appendix C. Note that the extracted hysteresis parameter is approximately a linear function of the vibration amplitude and hence the bias voltage amplitude, consistent with the observation of the earlier study [30].

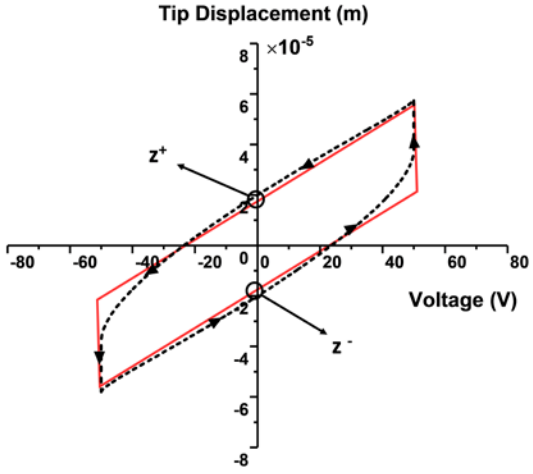

Fig. 4. The measured hysteresis loop (black dashed lines) for a bimorph piezoelectric actuator subject to 50 V sinusoidal voltage at 60 Hz (resonance frequency of the piezoelectric fan). The solid line shows a parallelogram approximating the hysteresis loop.

The hysteresis parameter H can also be estimated independently by fitting the frequency-dependence of the vibration amplitudes of harmonically excited actuators measured in vacuum using Eq. (3) with H as the free parameter in a genetic algorithm [33]. Representative data of the tip vibration amplitudes normalized with respect to the static tip deflection (δ_{static}) are shown in Fig. (5) as a function of the normalized actuation frequency. Here, ω_n is the first resonant frequency of the actuator. The values of H obtained using this method agree with the values obtained using the hysteresis curves discussed above to within 15%. Also shown for comparison are the curve fits obtained without accounting for mechanical hysteresis (Eq. (3) with $H = 0$). The frequency-dependence of vibrational amplitudes cannot be captured properly without considering mechanical hysteresis.

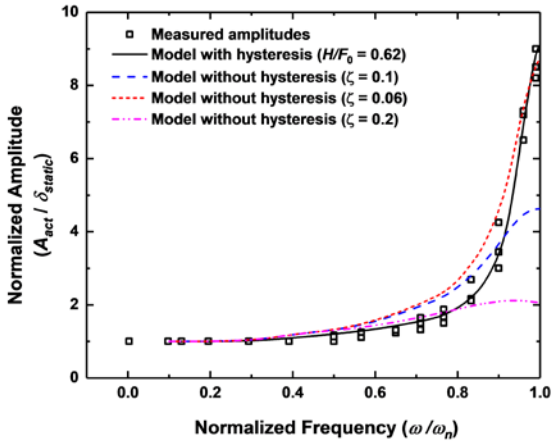

Fig. 5. The normalized tip vibration amplitudes in vacuum as a function of the normalized frequency for a piezoelectric bimorph actuator. The solid line represents the model predictions that account for mechanical hysteresis and the dashed, short-dashed, and dash-dotted lines show the model fit without accounting for the mechanical hysteresis. ξ is the damping factor used for each case.

The power consumption in the actuator can be calculated using the following expression:

$$P_{actuator} = 4H|A_{actuator}|f + V_{rms}^2\, Re(Y) + 2\pi^2 C_1 |A_{actuator}|^2 f^2 \qquad (4)$$

Here, $A_{actuator}$ is the vibration amplitude of the tip of the actuator and f is the vibration frequency. The last term represents dissipation due to structural damping, which is measured from damped free vibration of the actuator in vacuum. It accounts for less than 1% of power dissipation in the actuator (Appendix D).

Fig. (6) shows the experimentally measured and predicted power dissipation in the actuator. For a fixed applied voltage amplitude, the power dissipation increases nearly linearly with the frequency. At a relatively low voltage amplitude (60 V), the dielectric loss is negligible [27], [28] and the mechanical hysteresis loss dominates the total power dissipation. At a higher voltage

amplitude (100 V), the dielectric loss becomes more important. Under actuation conditions tested here, the mechanical hysteresis accounts for over 70% of the power dissipated in the actuators. The power dissipation predicted using our model agrees well with the experimental results. We emphasize that all the parameters used in the model, especially the hysteresis factor H and the dielectric loss factor $\tan\delta$, are obtained independently. Previous studies suggested approaches to reduce mechanical hysteresis loss [34][35][36].

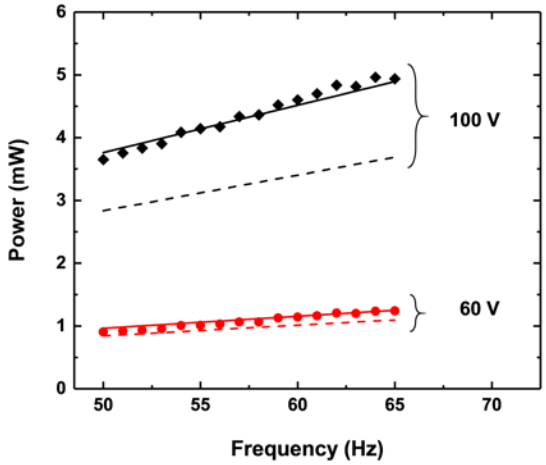

Fig. 6. Power dissipation in the piezoelectric actuator under different applied voltages: 60 V (red) and 100 V (black). The experimentally measured values are shown as the symbols, the predicted mechanical loss as the dashed lines, and the sum of the predicted mechanical and electrical losses as the solid lines.

3.2. Piezoelectric fans

We next extend our model to consider total power dissipation in piezoelectric fans equipped with flexible blades. Fig. (7) shows our mechanical model for a complete piezoelectric fan. Baker et al. [25] identified viscous dissipation in air flows generated by a vibrating beam as a major mechanism of power consumption in the system. For large-amplitude vibrations, where the tip displacements are comparable to the dimensions of the blade, previous studies ([25] [37]) showed that the rate of viscous dissipation is approximately proportional to the tip velocity squared. We note that structural damping of the blade measured in vacuum is responsible for less than 10% of typical total power consumption in the present study (Appendix D). In view of this, we neglect structural damping in the model as a separate source of dissipation for mathematical simplicity.

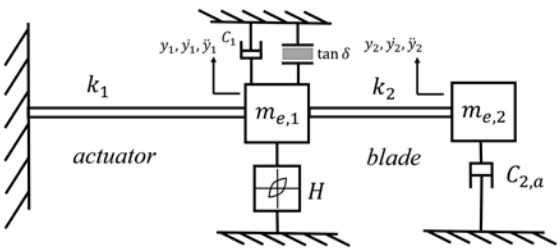

Fig. 7. Schematic of the mechanical model we use to describe a complete piezoelectric fan.

The equation of motion of the complete mechanical system is:

$$\begin{bmatrix} m_{e,1} & 0 \\ 0 & m_{e,2} \end{bmatrix} \begin{bmatrix} \ddot{y}_1 \\ \ddot{y}_2 \end{bmatrix} + \begin{bmatrix} C_1 & 0 \\ 0 & 0 \end{bmatrix} \begin{bmatrix} \dot{y}_1 \\ \dot{y}_2 \end{bmatrix} + \begin{bmatrix} 0 & 0 \\ 0 & C_{2,a} \end{bmatrix} \begin{bmatrix} \dot{y}_1|\dot{y}_1| \\ \dot{y}_2|\dot{y}_2| \end{bmatrix} + \begin{bmatrix} H & 0 \\ 0 & 0 \end{bmatrix} sign\left(\begin{bmatrix} \dot{y}_1 \\ \dot{y}_2 \end{bmatrix} \right) + \begin{bmatrix} (k_1 + k_2) & -k_2 \\ -k_2 & k_2 \end{bmatrix} \begin{bmatrix} y_1 \\ y_2 \end{bmatrix} =$$

$$\begin{bmatrix} F_0 \sin(\omega t) \\ 0 \end{bmatrix} \tag{5}$$

Here, $m_{e,2}$ is the effective mass of the blade, which is determined by transforming the distributed inertial force into a point force acting on the center of pressure [38], [39]. From the observation of negligible difference in resonance frequency between the ambient condition and vacuum, Bidkar et. al. [37] concluded that the added mass effect from air is negligible for typical piezoelectric fans.

The damping factor $C_{2,a}$ captures the aerodynamic damping of the blade vibration, which is a dominant source of power dissipation near the resonance. We fit the measured vibration amplitudes of the blades using Eq. (5) to determine C_{2a}. A representative result is illustrated in Fig. (8).

The rate of viscous dissipation, also referred to as the airflow power, is

$$P_{flow} = \frac{32\pi^2}{3} C_{2a} |A_{blade}|^3 f^3 \tag{6}$$

when averaged over one period. Here, A_{blade} is the vibration amplitude of the blade at its center of pressure and is linearly related to A_{tip}, the vibration amplitude at the tip of the blade.

Note that the blade tip velocity $u_{tip} = f A_{tip}$. The airflow power P_{flow} then scales as

$$P_{flow} \sim {u_{tip}}^3 \tag{7}$$

The total power dissipation in the piezoelectric fan is estimated by summing P_{flow} and $P_{actuator}$, while neglecting the structural damping of the actuator:

$$P_{total} = P_{actuator} + P_{flow} = 4H|A_{actuator}|f + V_{rms}^2 \, Re(Y) + \frac{32\pi^2}{3} C_{2a} |A_{blade}|^3 f^3 \tag{8}$$

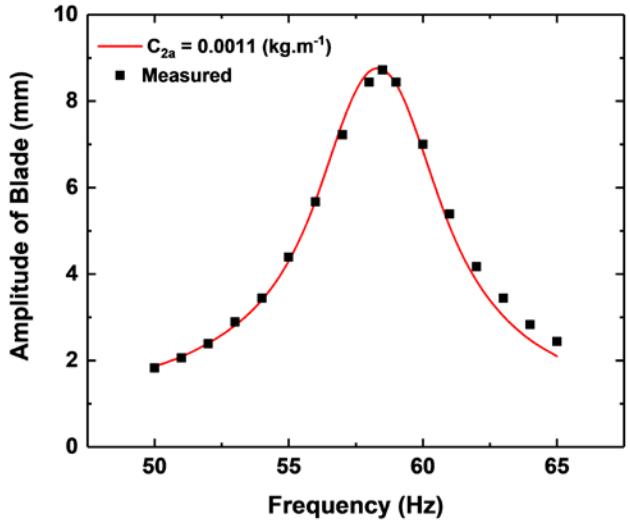

Fig. 8. A representative result showing the measured vibration amplitude at the blade tip as a function of the excitation frequency (the black symbols) and the fit with our mechanical model (the solid line).

Fig. (9) shows the experimentally measured and predicted power dissipation for a piezoelectric fan operating near its first resonance frequency. Also shown is the power dissipation in the actuator, which is obtained from a nominally identical piezoelectric fan but with its blade cut off. The applied voltage amplitude is 80 V.

Away from the resonance, the vibration amplitude of the blade tip is small. The power dissipation in the piezoelectric fan is then dominated by the mechanical hysteresis and dielectric loss in the actuator.

In contrast, at or near the resonance frequency (58 Hz), there is a peak in the power dissipation for the piezoelectric fan. The difference between the piezoelectric fan and the actuator (without the blade) can be accounted for by the airflow power, P_{flow}. It is this portion of the power dissipation that should correlate with the heat transfer performance. The total power dissipation predicted using Eq. (8) with independently determined parameters matches the experimental data well.

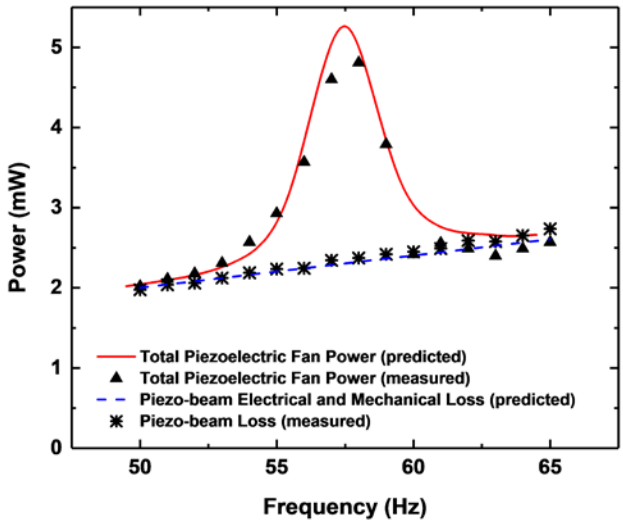

Fig. 9. Power dissipation in a piezoelectric fan and in a bare actuator (with the blade cut off). The measured powers (triangles) peak at the resonance frequency of the fan (~58 Hz). The predicted powers are also shown as the red solid line and the blue dashed line.

4. Heat Transfer Performance and Power Dissipation

To examine relationships between the heat transfer performance of piezoelectric fans and the power dissipation, specifically the airflow power, we perform several sets of experiments using piezoelectric fans of different geometric parameters (Table 1).

Fig. (10) shows the Nusselt numbers ($Nu_{total} = h_{total}L/k_{air}$) obtained from all the piezoelectric fans and the operating conditions summarized in Table 1. Here, L is the length of the heated surface and k_{air} is the thermal conductivity of air. The results from these piezoelectric fans and operating conditions correlate reasonably well with the airflow power.

At first glance, this result appears to suggest that changing the geometric parameters of the blade (length, thickness, and center of mass) has a limited effect on the power efficiency of the fans. That is, any enhancement in the heat transfer coefficient may need to be accompanied by corresponding increase in power dissipation. This is somewhat misleading, however, as the total power dissipation also includes contributions from the dielectric loss and mechanical loss as discussed in Section 3.

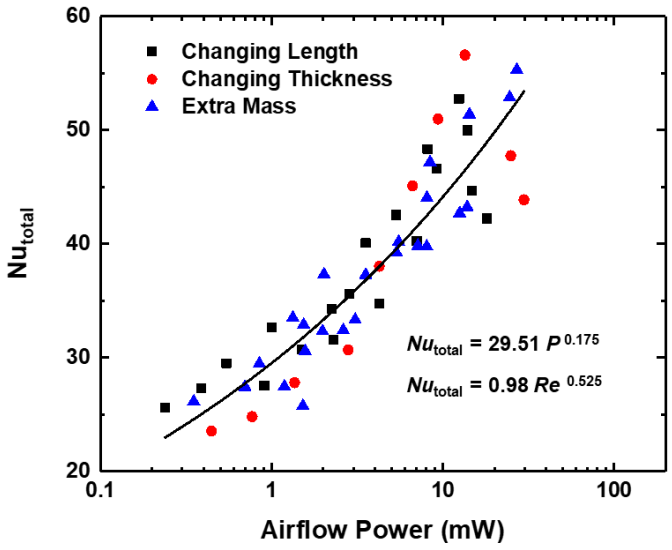

Fig. 10. The Nusselt number as a function of the airflow power for all the piezoelectric fans and operating conditions used in the present study. The solid line is a guide to the eye to illustrate a positive correlation between the heat transfer coefficient and the airflow power.

The data shown in Fig. (10) can be fitted using an empirical relation of the form

$$Nu_{total} \sim P_{flow}^{0.175} \tag{9}$$

Using Eq. (6) for P_{flow} and the Reynolds number defined in terms of the tip velocity u_{tip}

$$Re = \frac{u_{tip}\, L}{\nu}, \tag{10}$$

we can re-write the above correlation in terms of the two dimensionless parameters:

$$Nu_{total} \sim Re^{0.525} \tag{11}$$

The above correlation is consistent with those reported in [40] and [41] for heat transfer performance of jets impinging on a flat surface. These earlier correlations reveal similar dependence of Nu_{total} on Re, namely $Nu_{\text{total}} \sim Re^{a}$ with $0.4 < a < 0.8$.

Note that the experimental data from piezoelectric fans of different blade thicknesses deviate more from the general trend than those from the other fans. We suspect that this larger deviation may have to do with additional structural damping in the thicker blades. Blades of different thicknesses were prepared by bonding different layers of Kapton sheets together. This may have led to different degrees of structural damping in different blades, which was not taken into account in our model for power dissipation.

To further help elucidate the physical origin of the airflow power, we perform a separate set of experiments where we measure the normal force exerted on an opposing flat surface by airflows generated by the piezoelectric fan. The opposing surface is located in the same relative orientation with respect to and at the same distance from the fan as our heated surface. The general trend once again can be captured in terms of the Reynolds number (shown in Fig. (11)):

$$F \sim Re^{2.36} \tag{12}$$

This is again consistent with a correlation reported earlier for the thrust force exerted by piezoelectric fans, $F \sim A_{blade}^{\,2.38} f^{\,2.19}$ [5].

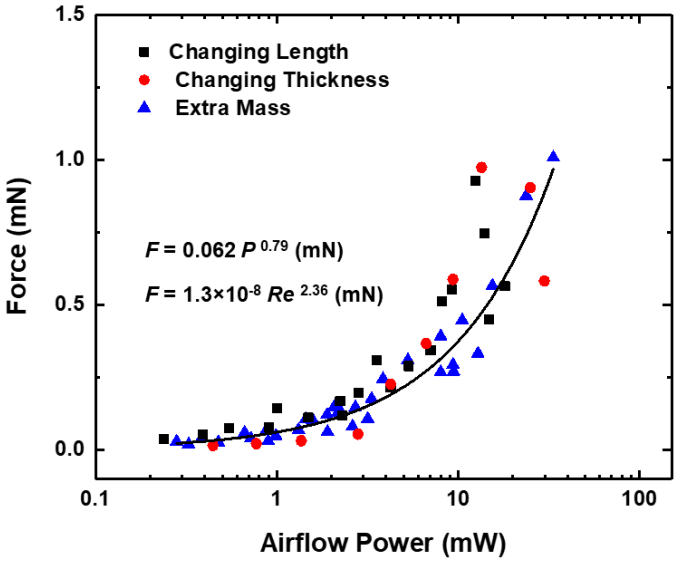

Fig. 11. The aerodynamic force exerted on an opposing surface by a piezoelectric fan as a function of the airflow power. The solid line is a guide to the eye to illustrate a positive correlation between the aerodynamic force and the airflow power.

Fig. (12) shows the airflow power as a function of the total power dissipation. For our particular set of fans, the airflow power accounts for approximately 30 to 80% of the total power dissipation. This fraction generally increases with increasing vibration frequencies because the airflow power exhibits stronger frequency-dependence than the dielectric and mechanical losses. Piezoelectric fans with longer blades, for example, can have worse overall power efficiencies than fans of shorter blades. However, merely trying to design a piezoelectric fan with a highest resonant frequency may lead to excessive reduction in the vibration amplitude of the blade tip, which can be detrimental to cooling performance.

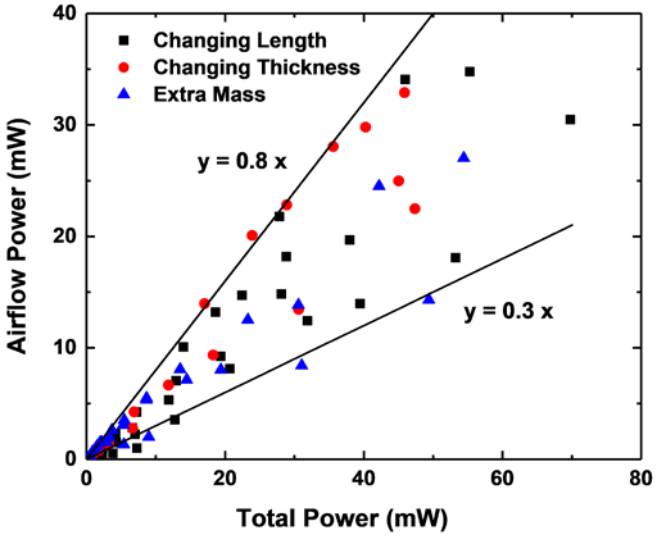

Fig. 12. Airflow power vs. total power consumption. Airflow power accounts for 30 to 80% of the total power dissipation in the piezoelectric fan.

A useful figure of merit for characterizing the power efficiency of piezoelectric fans is the ratio between the flow power P_{flow} and the total power P_{total}. This ratio is represented as the slope in Fig. 12. The ratio, hereafter referred to as the cooling power efficiency, can be expressed using parameters from our power dissipation model as

$$\frac{P_{flow}}{P_{total}} = \frac{\frac{32\pi^2}{3} C_{2a} |A_{blade}|^3 f^3}{4H|A_{actuator}|f + V_{rms}^2 \, Re(Y) + \frac{32\pi^2}{3} C_{2a} |A_{blade}|^3 f^3} \tag{13}$$

Since the airflow power has the strongest frequency dependence, we expect the cooling power efficiency increases as the frequency increases. To help explore the bias voltage amplitude dependence of the cooling power efficiency, we represent those parameters in the above equation that depend on the bias voltage amplitude V as

$$A_{actuator} = C_{act} V \tag{14}$$

$$A_{blade} = C_{blade} \, A_{actuator} = (C_{blade} \, C_{act}) V \tag{15}$$

$$H = C_H V \tag{16}$$

$$Re(Y) = C_Y V^2 f \tag{17}$$

$$V_{rms} = \frac{\sqrt{2}}{2} V \tag{18}$$

The coefficients C_{act}, C_{blade}, C_{H} and C_{Y} are determined either experimentally or obtained from literature. Note that parameters A_{actuator}, A_{blade}, C_{H} and $\tan\delta$ (via Y) in Eqs. (14) – (17) are assumed to be independent of the actuation frequency under the conditions of our experiments [27].

The cooling power efficiency can then be rewritten as

$$\frac{P_{flow}}{P_{total}} = \frac{\overbrace{\left[\frac{32\pi^2}{3} C_{2a} C_{blade}{}^3 C_{act}{}^3\right]}^{\alpha} V^3 f^3}{\underbrace{[4C_H C_{act}]}_{\beta} V^2 f + \underbrace{\left[\frac{C_Y}{2}\right]}_{\gamma} V^4 f + \underbrace{\left[\frac{32\pi^2}{3} C_{2a} C_{blade}{}^3 C_{act}{}^3\right]}_{\alpha} V^3 f^3} \tag{19}$$

Here, the parameter group α captures the aerodynamic and geometrical properties of the blade, the group β mechanical loss in the actuator, and the group γ dielectric loss in the actuator.

Fig. (13) shows the cooling power efficiency as a function of the bias voltage amplitude V for five different actuation frequencies. For each actuation frequency, the cooling power efficiency exhibits a peak value. To the left of these peaks, the blade vibration

amplitude and the air flow power are small. The mechanical hysteresis loss, which scales as V^2, is the dominant source of power dissipation in this region. Since the air flow power scales as V^3, the cooling power efficiency first increases with increasing bias voltage amplitudes. As the bias voltage amplitude is increased further, the dielectric loss, which scales as V^4, becomes more significant. The increase in the air flow power cannot keep up with the increase in the dielectric loss and the cooling power efficiency begins to decrease with further increase in the bias voltage amplitude. At still higher values of V, the amplitude of blade vibration tends to saturate while the airflow power stays almost constant, leading to a further gradual decrease in the cooling power efficiency. This decrease is more pronounced at lower actuation frequencies.

The bias voltage amplitude where the maximum cooling power efficiency occurs is mathematically obtained by equating the first derivative of Eq. (19) with respect to V to zero:

$$V_{max} = \sqrt{\frac{\beta}{\gamma}} \tag{20}$$

For the piezoelectric actuators used in the present study, we estimate V_{max} to be 101 V. The data shown in Fig. 12 with the high cooling power efficiencies (as high as 0.8) are obtained with bias voltages 90 ~ 120 V, consistent with this value of V_{max}. Note that this voltage amplitude only depends on β and γ, which in turn depend only on the geometry and material properties of the actuator and not those of the blade or actuation frequency. Although V_{max} itself is a function only of the actuator characteristics, the value of the maximum cooling power efficiency is a function of the blade characteristics and actuation frequency:

$$\left(\frac{P_{flow}}{P_{total}}\right)_{max} = \frac{\alpha\left(\frac{\beta}{\gamma}\right)^{3/2} f^3}{2\frac{\beta^2}{\gamma} f + \alpha\left(\frac{\beta}{\gamma}\right)^{3/2} f^3} \tag{21}$$

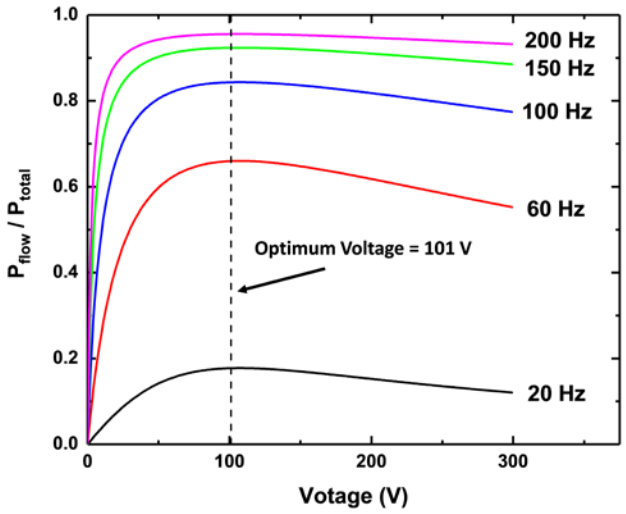

Fig. 13. The cooling power efficiency obtained from our model as a function of the bias voltage amplitude at different frequencies. Note that the voltage amplitude that corresponds to the peaks in the cooling power efficiency does not change with the frequency over the range considered in the present work.

In designing or selecting piezoelectric fans, one must consider both the power efficiency and the absolute heat transfer performance, which we have shown to correlate with the air flow power. To facilitate such design processes, we next present an approximate relation between the air flow power and the geometric parameters of fan blades.

We first rewrite Eq. (6) explicitly in terms of the blade parameters. The resonance frequency is first expressed as [38], [39]:

$$f_{res.} \sim \left(\frac{E}{\rho_{blade}}\right)^{0.5} \frac{t_b}{l_b^2} \tag{22}$$

The aerodynamic damping coefficient, $C_{2,a}$ is linearly proportional to the area of the blade, lw [37]:

$$C_{2,a} \sim \rho_{air}\, l_b w_b \tag{23}$$

The amplitude of the blade is linearly dependent on the amplitude of the actuator tip (Eq. (15)). From the experimental data and mathematical model (Fig. (7) and Eq. (5)), we relate C_{blade} with the mass densities:

$$C_{blade} \sim \left(\frac{\rho}{\rho_{air}}\right)^{0.5} \tag{24}$$

Substituting Eqs. (22) – (25) into Eq. (6), we obtain:

$$P_{flow} = C^* \frac{E^{1.5}}{\rho_{air}{}^{0.5}} \left\{\frac{w_b\, t_b^3}{l_b^5}(C_{act}V)^3\right\} \tag{25}$$

where C^* is a proportionality constant.

We compare the air flow powers we extract from the experimental data with the predicted trend from Eq. (25) to determine the proportionality constant, C^*, for our piezoelectric fans. The experimental values and the fit are shown in Fig. 14. Given that the air flow power is obtained indirectly and has appreciable uncertainty, we consider the quality of the fit to be overall reasonable. We note that the model represented in Eq. (25) does not account for possible non-linearity in the mechanical behavior of blades and their structural damping.

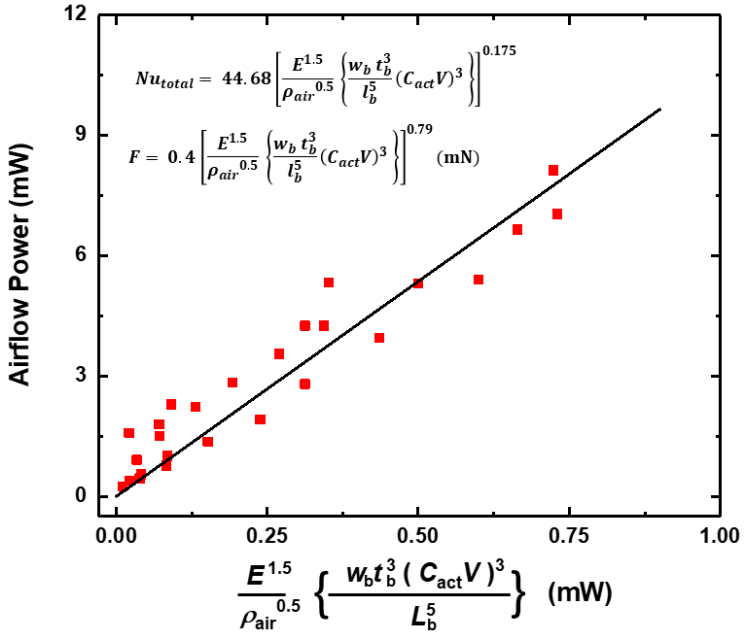

Fig. 14. A linear fit to the air flow power obtained from the experiments (red symbols) to determine the proportionality constant C^* (10.7) in Eq. (25). The average deviation between the data and the curve fit is approximately 25% of the mean value of the airflow power over the range considered. Approximate analytic expressions for the heat transfer coefficient and the normal aerodynamic force on an opposing surface may be obtained in terms of the geometrical parameters of the blades by substituting Eq. (25) into the least-square fits to the experimental data: GIVE EQUATIONS HERE . The average deviation between the data and the fit is approximately 10% (for the heat transfer coefficient) and 20% (for the aerodynamic force) of the respective mean value.

5. CONCLUSION

Optimizing the power efficiency of piezoelectric fans requires a deeper understanding of the mechanisms involved in their power consumption. We report a combined experimental and modeling study to help elucidate different power dissipation mechanisms in piezoelectric fans and obtain an optimal operating condition for maximum power efficiency. We measure power dissipation in fans of different blade lengths, thicknesses and mass distributions as functions of the frequency and magnitude of sinusoidal bias voltages. Models that account for dielectric loss, mechanical hysteresis, and aerodynamic damping from generated air flows are used to partition power dissipated in the fans.

Our data and model analyses show that the mechanical hysteresis loss and, to a lesser extent, the dielectric loss are dominant sources of parasitic power dissipation in the actuators. Our measurements show that 30 to 80% of the total power consumed stem for generated air flows. The experimentally determined average heat transfer coefficients and aerodynamic thrust forces on flat surfaces correlate generally well with the air flow power, further verifying the fluid dynamics origin of this portion of dissipated power.

We introduce the power ratio as a useful indicator of the portion of total power that is used to generate air flows and thereby contributes to convective cooling. Using our mechanical models, we investigate the frequency and voltage dependence of the

power ratio and determine an optimal bias voltage amplitude that maximizes the power ratio by balancing the mechanical hysteresis loss and the dielectric loss with respect to the air flow power.

Finally, we relate the air flow power and hence heat transfer performance to the blade's geometrical parameters to assist overall design or selection of fan blades.

The present work helps improve our understanding of the power consumption in piezoelectric fans and thereby facilitate their more systematic optimization.

6. Acknowledgement

The present article is based in part on work supported by the Advanced Research Projects Agency-Energy (ARPA-E) under Award No. DE-AR0000532.

References

[1] M. Arik, J. Petroski, A. Bar-Cohen, and M. Demiroglu, "Energy Efficiency of Low Form Factor Cooling Devices," pp. 1347–1354, Jan. 2007.

[2] M. Kimber, K. Suzuki, N. Kitsunai, K. Seki, and S. V. Garimella, "Pressure and Flow Rate Performance of Piezoelectric Fans," *IEEE Trans. Compon. Packag. Technol.*, vol. 32, no. 4, pp. 766–775, Dec. 2009.

[3] T. Açikalin and S. V. Garimella, "Analysis and Prediction of the Thermal Performance of Piezoelectrically Actuated Fans," *Heat Transf. Eng.*, vol. 30, no. 6, pp. 487–498, May 2009.

[4] Y.-H. Kim, S. T. Wereley, and C.-H. Chun, "Phase-resolved flow field produced by a vibrating cantilever plate between two endplates," *Phys. Fluids 1994-Present*, vol. 16, no. 1, pp. 145–162, Jan. 2004.

[5] A. Eastman, J. Kiefer, and M. Kimber, "Thrust measurements and flow field analysis of a piezoelectrically actuated oscillating cantilever," *Exp. Fluids*, vol. 53, no. 5, pp. 1533–1543, Sep. 2012.

[6] A. Eastman and M. L. Kimber, "Aerodynamic damping of sidewall bounded oscillating cantilevers," *J. Fluids Struct.*, vol. 51, pp. 148–160, Nov. 2014.

[7] M. Kimber, S. V. Garimella, and A. Raman, "An Experimental Study of Fluidic Coupling Between Multiple Piezoelectric Fans," in *Thermal and Thermomechanical Proceedings 10th Intersociety Conference on Phenomena in Electronics Systems, 2006. ITHERM 2006.*, 2006, pp. 333–340.

[8] C.-N. Lin, "Analysis of three-dimensional heat and fluid flow induced by piezoelectric fan," *Int. J. Heat Mass Transf.*, vol. 55, no. 11–12, pp. 3043–3053, May 2012.

[9] T. Lei, Z. Jing-zhou, and T. Xiao-ming, "Numerical investigation of convective heat transfer on a vertical surface due to resonating cantilever beam," *Int. J. Therm. Sci.*, vol. 80, pp. 93–107, Jun. 2014.

[10] T. AÇIKALIN, S. M. WAIT, S. V. GARIMELLA, and A. RAMAN, "Experimental Investigation of the Thermal Performance of Piezoelectric Fans," *Heat Transf. Eng.*, vol. 25, no. 1, pp. 4–14, Jan. 2004.

[11] S. F. Sufian, M. Z. Abdullah, M. K. Abdullah, and J. J. Mohamed, "Effect of Side and Tip Gaps of a Piezoelectric Fan on Microelectronic Cooling," *IEEE Trans. Compon. Packag. Manuf. Technol.*, vol. 3, no. 9, pp. 1545–1553, Sep. 2013.

[12] P. Burmann, A. Raman, and S. V. Garimella, "Dynamics and topology optimization of piezoelectric fans," *IEEE Trans. Compon. Packag. Technol.*, vol. 25, no. 4, pp. 592–600, Dec. 2002.

[13] T. Wu, P. I. Ro, A. I. Kingon, and J. F. Mulling, "Piezoelectric resonating structures for microelectronic cooling," *Smart Mater. Struct.*, vol. 12, no. 2, p. 181, 2003.

[14] T. Açıkalın, S. V. Garimella, A. Raman, and J. Petroski, "Characterization and optimization of the thermal performance of miniature piezoelectric fans," *Int. J. Heat Fluid Flow*, vol. 28, no. 4, pp. 806–820, Aug. 2007.

[15] J. Cho, T. Lim, and B. S. Kim, "Measurements and predictions of the air distribution systems in high compute density (Internet) data centers," *Energy Build.*, vol. 41, no. 10, pp. 1107–1115, Oct. 2009.

[16] J. H. Yoo, J. I. Hong, and W. Cao, "Piezoelectric ceramic bimorph coupled to thin metal plate as cooling fan for electronic devices," *Sens. Actuators Phys.*, vol. 79, no. 1, pp. 8–12, Jan. 2000.

[17] C.-H. Huang, Y.-F. Chen, and H. Ay, "An inverse problem in determining the optimal position for piezoelectric fan with experimental verification," *Int. J. Heat Mass Transf.*, vol. 55, no. 19–20, pp. 5289–5301, Sep. 2012.

[18] C.-H. Huang and G.-Y. Fan, "Determination of relative positions and phase angle of dual piezoelectric fans for maximum heat dissipation of fin surface," *Int. J. Heat Mass Transf.*, vol. 92, pp. 523–538, Jan. 2016.

[19] J. Petroski, M. Arik, and M. Gursoy, "Optimization of Piezoelectric Oscillating Fan-Cooled Heat Sinks for Electronics Cooling," *IEEE Trans. Compon. Packag. Technol.*, vol. 33, no. 1, pp. 25–31, Mar. 2010.

[20] R. R. Schmidt, "Local and average transfer coefficients on a vertical surface due to convection from a piezoelectric fan," in , *InterSociety Conference on Thermal Phenomena in Electronic Systems, 1994. I-THERM IV. Concurrent Engineering and Thermal Phenomena*, 1994, pp. 41–49.

[21] C. Liang, F. P. Sun, and C. A. Rogers, "An Impedance Method for Dynamic Analysis of Active Material Systems," *J. Vib. Acoust.*, vol. 116, no. 1, pp. 120–128, Jan. 1994.

[22] Y. S. Cho, Y. E. Pak, C. S. Han, and S. K. Ha, “Five-port equivalent electric circuit of piezoelectric bimorph beam,” *Sens. Actuators Phys.*, vol. 84, no. 1–2, pp. 140–148, Aug. 2000.
[23] S. M. Wait, S. Basak, S. V. Garimella, and A. Raman, “Piezoelectric Fans Using Higher Flexural Modes for Electronics Cooling Applications,” *IEEE Trans. Compon. Packag. Technol.*, vol. 30, no. 1, pp. 119–128, Mar. 2007.
[24] W.-J. Sheu, R.-T. Huang, and C.-C. Wang, “Influence of bonding glues on the vibration of piezoelectric fans,” *Sens. Actuators Phys.*, vol. 148, no. 1, pp. 115–121, Nov. 2008.
[25] W. E. Baker, W. E. Woolam, and D. Young, “Air and internal damping of thin cantilever beams,” *Int. J. Mech. Sci.*, vol. 9, no. 11, pp. 743–766, Nov. 1967.
[26] “IEEE Standard on Piezoelectricity,” *ANSIIEEE Std 176-1987*, p. 0_1-, 1988.
[27] M. W. Hooker, “Properties of PZT-Based Piezoelectric Ceramics Between -150 and 250 C,” Sep. 1998.
[28] A. I. Kingon, P. J. Terblanche, and J. B. Clark, “Variability of the high field properties of PZT-4 and PZT-8 type piezoelectric ceramics,” *Ferroelectrics*, vol. 37, no. 1, pp. 635–638, Oct. 1981.
[29] T. S. Low and W. Guo, “Modeling of a three-layer piezoelectric bimorph beam with hysteresis,” *J. Microelectromechanical Syst.*, vol. 4, no. 4, pp. 230–237, Dec. 1995.
[30] M. Rakotondrabe, Y. Haddab, and P. Lutz, “Quadrilateral Modelling and Robust Control of a Nonlinear Piezoelectric Cantilever,” *IEEE Trans. Control Syst. Technol.*, vol. 17, no. 3, pp. 528–539, May 2009.
[31] W. T. Ang, F. A. Garmon, P. K. Khosla, and C. N. Riviere, “Modeling rate-dependent hysteresis in piezoelectric actuators,” in *Proceedings 2003 IEEE/RSJ International Conference on Intelligent Robots and Systems (IROS 2003) (Cat. No.03CH37453)*, 2003, vol. 2, pp. 1975–1980 vol.2.
[32] G. Bertotti and I. D. Mayergoyz, *The Science of Hysteresis: Hysteresis in materials*. Gulf Professional Publishing, 2006.
[33] D. Whitley, “A genetic algorithm tutorial,” *Stat. Comput.*, vol. 4, no. 2, pp. 65–85, Jun. 1994.
[34] S. Chonan, Z. Jiang, and T. Yamamoto, “Nonlinear Hysteresis Compensation of Piezoelectric Ceramic Actuators,” *J. Intell. Mater. Syst. Struct.*, vol. 7, no. 2, pp. 150–156, Mar. 1996.
[35] A. J. Fleming and S. O. R. Moheimani, “A grounded-load charge amplifier for reducing hysteresis in piezoelectric tube scanners,” *Rev. Sci. Instrum.*, vol. 76, no. 7, p. 73707, Jun. 2005.
[36] J. Minase, T.-F. Lu, B. Cazzolato, and S. Grainger, “A review, supported by experimental results, of voltage, charge and capacitor insertion method for driving piezoelectric actuators,” *Precis. Eng.*, vol. 34, no. 4, pp. 692–700, Oct. 2010.
[37] R. A. Bidkar, M. Kimber, A. Raman, A. K. Bajaj, and S. V. Garimella, “Nonlinear aerodynamic damping of sharp-edged flexible beams oscillating at low Keulegan–Carpenter numbers,” *J. Fluid Mech.*, vol. 634, pp. 269–289, 2009.
[38] M. Toda, “Theory of air flow generation by a resonant type PVF2 bimorph cantilever vibrator,” *Ferroelectrics*, vol. 22, no. 1, pp. 911–918, Jan. 1978.
[39] K. Yao and K. Uchino, “Analysis on a composite cantilever beam coupling a piezoelectric bimorph to an elastic blade,” *Sens. Actuators Phys.*, vol. 89, no. 3, pp. 215–221, Apr. 2001.
[40] K. Jambunathan, E. Lai, M. A. Moss, and B. L. Button, “A review of heat transfer data for single circular jet impingement,” *Int. J. Heat Fluid Flow*, vol. 13, no. 2, pp. 106–115, 1992.
[41] J. C. AKFIRAT, “Heat transfer characteristics of impinging two-dimensional air jets,” 1966.

Navid Dehdari Ebrahimi received his B.Sc. in mechanical engineering from Sharif University of Technology, Iran in 2015. He is currently a PhD Candidate at University of California, Los Angeles (UCLA). His research is mainly focused on power consumption optimization of piezoelectric fans for micro and mesoscale cooling enhancement.

Yide Wang received his B.Sc. and M.Sc. in mechanical engineering from Purdue University in 2015 and University of California, Los Angeles in 2017 respectively. He is currently pursuing a PhD degree from UCLA, working on system level performance study of thermal energy storage system with sulfur as storage medium.

Professor Y. Sungtaek Ju Received his PhD in Mechanical Engineering from Stanford University in 1999. Prof. Ju worked as a research staff member at IBM before joining the UCLA faculty. He is currently the head of MTSLab at UCLA. His current research interests are in MEMS/Nanotechnology, especially its applications to the thermal management of electronics and buildings; energy conversion technologies; and water-energy nexus.

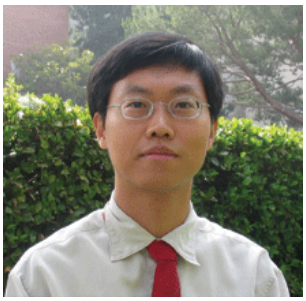

APPENDIX

A. NOMENCLATURE

A_{act}	Amplitude of the actuator, m	$P_{dielectric}$	Dielectric loss in the actuator, mW
A_{blade}	Amplitude of the blade, m	P_{flow}	Airflow power, mW
C_1	Structural damping of the actuator, kg/s	P_{total}	Total power consumption of the fan, mW
$C_{2,a}$	Aerodynamic damping of the blade, kg/m	Q_{heater}	Heater Power, W
C_{act}	Actuator coefficient, m/V	Q_{loss}	Heat loss, W
C_{blade}	Blade coefficient, dimensionless	Re	Reynolds number, dimensionless
C_H	Hysteresis coefficient, N/V	Re(Y)	Real part of the actuator admittance, 1/Ω
C_Y	Dielectric loss coefficient, J/V^4	S	Area of the heated surface, m^2
d	Location of the added mass, m	T	Period of oscillations, s
d_e	Piezoelectric displacement factor, m/V	t	Time, s
E	Young's modulus, GPa	t_b	Thickness of the blade, mm
F	Force on an opposing surface, mN	$tan\delta$	Tangent loss factor of the actuator, dimensionless
F_0	Equivalent force at the tip of the actuator, N	u_{tip}	Blade tip velocity, fA_{blade}, m/s
f	Frequency, Hz	V	Amplitude of the bias voltage, V
H	Hysteresis factor, N	V_{max}	Bias voltage for maximum efficiency, V
h_{total}	Total (free and forced) convection heat transfer coefficient, W/m^{2}K	V_{rms}	RMS voltage, V
k_1	Bending stiffness of the actuator, N/m	w_b	Width of the blade, m
k_2	Bending stiffness of the blade, N/m	z	State variable, m
k_{air}	Thermal conductivity of air, W/mK	**Greek symbols**	
L	Length of the heated surface, mm	α	Aerodynamic and geometrical parameter, J s^2/V^3
l_b	Length of the blade, mm	α_p	Parameter related to the shape of the hysteresis curve, dimensionless
l_p	Length of the actuator, mm	β	Mechanical loss parameter, J /V^2
m_0	Original mass, kg	β_p	Parameter related to the shape of the hysteresis curve, dimensionless
$m_{e,1}$	Effective mass of the actuator, kg	γ	Hysteresis loss parameter, J /V^4
$m_{e,2}$	Effective mass of the blade, kg	γ_p	Parameter related to the shape of the hysteresis curve, dimensionless
Nu_{total}	Total (free and forced) Nusselt number, dimensionless	ω	Angular frequency, rad/s
$P_{actuator}$	Power consumption in the actuator, mW		

B. HYSTERESIS APPROXIMATION

We substitute V in Eq. (2) with a sinusoidal signal, $V = V_0 \sin(\omega t)$ and solve the first equation for the state variable z using representative values of α, β and γ reported in a previous study for piezoelectric actuators [29]. The predicted temporal variation in z, shown in Fig. (B.1), can be approximated with a step function, that is, a constant value with alternating signs tracking $\cos(\omega t)$, or the direction of the oscillation velocity. Based on these results, we approximate the term $k_1 z$ in Eq. (2) with $H\ sign(\dot{y})$ for mathematical simplicity.

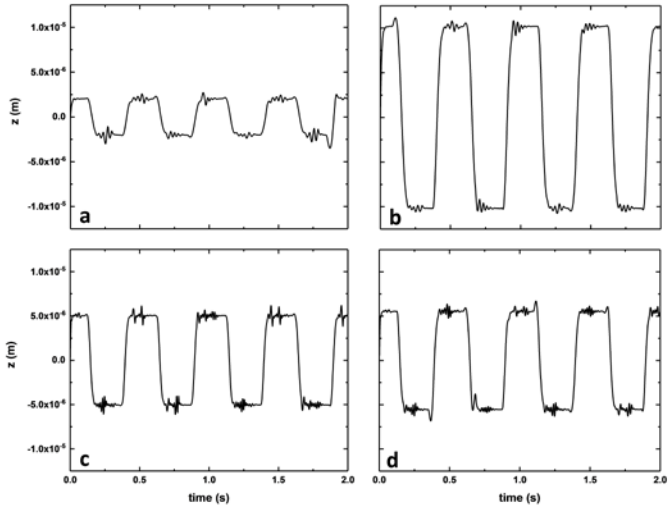

Fig. B.1. Calculated values of z for a sinusoidal excitation voltage with a) α=1×10 $^{-1}$, β=5×10 $^{-2}$, γ=-1×10 $^{-3}$, d_e=1×10 $^{-6}$ b) α=5×10^{-1}, β=5×10 $^{-2}$, γ=-1×10^{-3}, d_e=1×10 $^{-6}$ c) α=5×10 $^{-1}$, β=1×10 $^{-1}$, γ=-1×10 $^{-3}$, d_e=1×10 $^{-6}$ d) α=5×10 $^{-1}$, β=1×10 $^{-1}$, γ=-1×10 $^{-2}$, d_e=1×10 $^{-6}$

C. DETERMINATION OF HYSTERESIS PARAMETER H USING HYSTERESIS LOOP

To determine the hysteresis parameter, H, we experimentally obtain hysteresis loops of our piezoelectric actuators. Figs. (C.1) – (C.3) show example hysteresis loops we obtain from our piezoelectric actuators for 3 different bias voltage amplitudes (50 V, 70 V, 120 V). Each loop is approximated using a parallelogram. The intersections of the parallel top and bottom sides with the displacement axis, labeled z^+ and z^-, are obtained and averaged ($\bar{z}$). The hysteresis parameter is then calculated as $H = k_1 \bar{z}$, The values thus obtained are normalized with the corresponding equivalent tip bending force F_0 and listed in table C.1 together with values reported in the literature for comparison. Measurements performed at two different actuation frequencies, 60 Hz and 150 Hz, show relatively small frequency dependence of the hysteresis parameter.

TABLE C.1
H PARAMETER (IN N) OBTAINED FROM HYSTERESIS LOOPS

	50 V	70 V	120 V	$H_{ave.}/F_0$	Literature
60 Hz	0.039	0.062	0.092	0.46	0.4 [30]
150 Hz	0.041	0.074	0.095	0.48	0.51 [30]

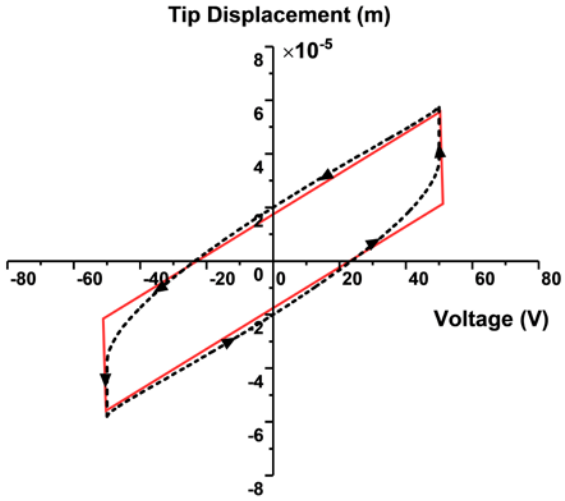

Fig. C.1. A measured hysteresis loop under 50 V sinusoidal voltage at 60 Hz.

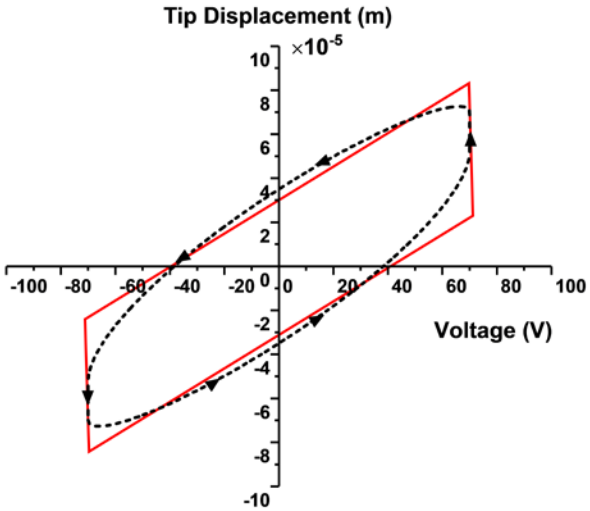

Fig. C.2. A measured hysteresis loop under 70 V sinusoidal voltage at 60 Hz.

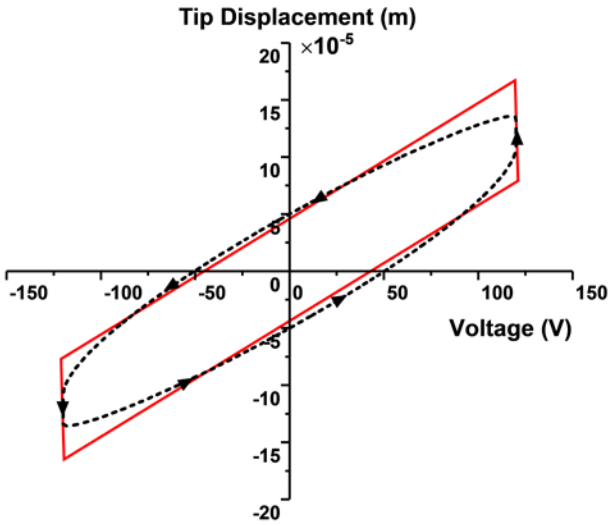

Fig. C.3. A measured hysteresis loop under 120 V sinusoidal voltage at 60 Hz.

D. Structural Damping of the Actuator and Blade

To determine power dissipation due to structural damping in piezoelectric actuators, we measure the step response of actuators under vacuum. We apply and then turn off a sinusoidal bias voltage of amplitude 100 V to an actuator. The resulting damped oscillations are then recorded and fitted with Eq. (3) to characterize structural damping. The average damping coefficient of 0.072 kg/s, thus obtained, translates into a relatively small power consumption of ~ 0.05 mW.

Using a similar procedure, we also characterize the structural damping of blades in the piezoelectric fans. The associated power consumption is again relatively small, approximately 0.5 mW.